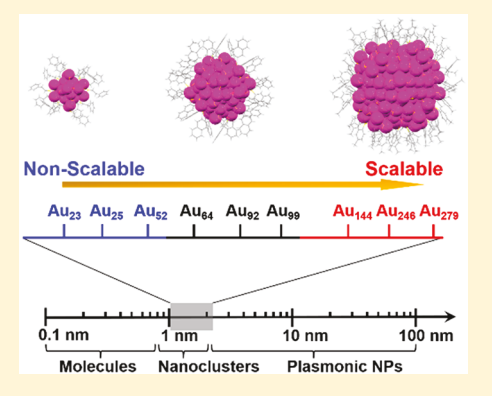


Three-Stage Evolution from Nonscalable to Scalable Optical **Properties of Thiolate-Protected Gold Nanoclusters**

Meng Zhou, †, Tatsuya Higaki, †, Pingwei Li, †, Chenjie Zeng, Qi Li, Matthew Y. Sfeir, *, © and Rongchao Jin*,†®

Supporting Information

ABSTRACT: The evolution of the optical properties of gold nanoclusters (NCs) versus size is of great importance because it not only reveals the nature of quantum confinement in NCs, but also helps to understand how the molecularlike Au NCs transit to plasmonic nanoparticles. While some work has been done in studying the optical properties of NCs of certain individual sizes, the global picture remains unclear, such as the detailed relationship between size/structure and properties. Here, we investigate the grand evolution of the optical properties by comparing the steady-state absorption, bandgap, transient absorption, as well as carrier dynamics of a series of thiolate-protected gold NCs ranging from tens to hundreds of gold atoms. We find that, on the basis of their optical behaviors, gold NCs can be classified into three groups: (i) ultrasmall NCs (ca. <50 Au atoms) are nonscalable as their optical properties are strongly dependent on the structure rather than size; (ii) medium-sized NCs (about 50-100 Au atoms) show both size- and structure-dependent optical properties; and (iii) large-sized



gold NCs (ca. >100 Au atoms) exhibit optical properties solely dependent on size, and the structure effect fades out. Unraveling the grand evolution from nonscalable to scalable optical properties and their mechanisms will greatly deepen scientific understanding of the nature of quantum-sized gold NCs and will also provide implications for plasmonic NPs.

1. INTRODUCTION

The optical absorption and scattering by metal nanoparticles (NPs) are dominated by surface plasmon resonance (SPR), which depends on the size, shape, composition, and surrounding environment.^{1,2} According to Mie's theory,³ the absorption and scattering spectra of metal NPs can be calculated with the dielectric constants of the particle material and the environment. Ultrasmall metal NPs, commonly called nanoclusters (NCs), start to exhibit quantized electronic energy bands and accordingly multiple discrete absorption peaks.4 It took major efforts to control metal NCs with atomic precision. With the success in atomically precise nanochemistry, such NCs have emerged as a new, unique class of materials with wide tunability, which have attracted significant research interest in both fundamental studies and developments of applications. 4-11 Among the physical properties, the optical properties of metal NCs have received great research interest because of the structure-enabled understanding and manipulation of such properties at the atomic level. 12-15 The optical absorption of NCs is closely related to their structures, and theoretical simulations based on structures have contributed greatly to the understanding of optical absorption. 16,17

Thiolate-protected Au NCs $(Au_n(SR)_m$ for short) constitute a paradigm system, and their structures typically comprise a metal core and staple-like surface motifs (containing both surface Au atoms and SR ligands).4 The presence of staple motifs leads to complicated optical properties due to the fact that both the metal core and surface staple motifs contribute to the frontier molecular orbitals. 15 The strong quantum confinement in small gold NCs (such as the Au₂₅ system) makes their optical properties very sensitive to a small change in the structure and/or composition. Indeed, a subtle change in structure or single atom replacement gives rise to a large change in the UV-vis absorption and other optical properties such as luminescence and excited-state dynamics; 18-23 thus, the optical properties in the small size regime are distinctly nonscalable. As the size becomes larger (e.g., more than 100 Au atoms), the quantum confinement becomes weaker and the absorption peaks also become crowded or overlapped and hence less prominent.²⁴ For such large sizes, changing the surface ligand or core structure would be less likely to induce drastic changes in the optical absorption spectra.²⁴

Received: August 21, 2019 Published: December 6, 2019



Department of Chemistry, Carnegie Mellon University, Pittsburgh, Pennsylvania 15213, United States

[‡]Photonics Initiative, Advanced Science Research Center, City University of New York, New York, New York 10031, United States

[§]Department of Physics, Graduate Center, City University of New York, New York, New York 10016, United States

Journal of the American Chemical Society

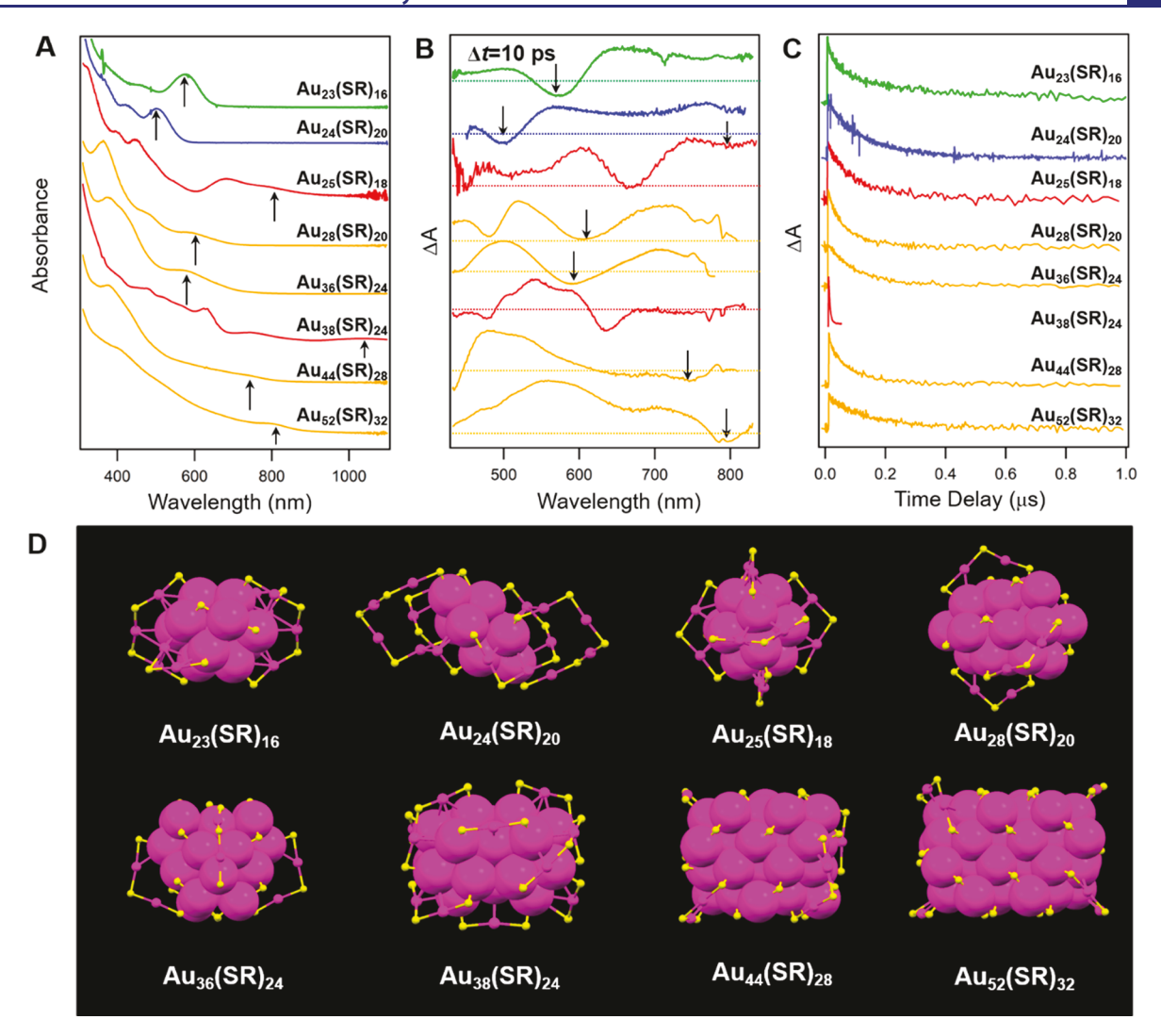


Figure 1. (A) UV–vis absorption spectra of a series of gold NCs. The lowest absorption peaks are marked with arrows. (B) Transient absorption spectra probed at 10 ps with 360 nm excitation. The GSBs from the lowest absorption peak are marked with arrows. (C) Kinetic decay obtained from nanosecond time-resolved transient absorption spectroscopy. (D) Crystal structure of these $Au_n(SR)_m$ samples. Carbon tails are omitted for clarity. Color labels: magenta = $Au_n(SR)_m$ samples.

Much effort has been made to study the optical properties of some individual sizes of Au_n(SR)_m. Back in 2008, Jin and coworkers for the first time correlated the optical absorption of the Au₂₅ nanocluster with its structure. 15 Tsukuda et al. studied the photoluminescence of a series of gold NCs, ²⁶ as well as the absorption and structure evolution in gold NCs. ^{26,27} Aikens et al. performed theoretical calculations on the excited states and photoluminescence of gold NCs. ^{28–30} Pei and Jiang et al. also investigated the optical property evolution in different types of structures by theoretical calculations. 17,31-33 Häkkinen and Lopez-Acevedo et al. theoretically simulated the optical absorption of a series of large gold NCs. 34,35 Goodson et al. investigated the optical properties of five different-sized NCs and found that the critical size for the emergence of molecular behavior is <2.2 nm. ³⁶ Ramakrishna et al. studied the nonlinear optical properties and electron-phonon coupling in different gold NCs. 12,37,38 Knappenberger et al. used multiple timeresolved spectroscopy methods to understand the different excited states in Au₂₅ NCs.^{39–41} Pettersson et al. probed the electron dynamics of Au₁₀₂ and Au₁₄₄ NCs using mid-IR pump—probe spectroscopy.^{42,43} Stamplecoskie et al. investigated the size-dependent carrier dynamics of water-soluble

Au_n NCs (n=10-12, 15, 18, 25) and also probed their photocatalytic activity. Aie et al. identified a highly luminescent Au₂₂ nanocluster (QY = 8%) and explained the mechanism as aggregation-induced emission. Lee et al. further increased the quantum yield of Au₂₂ to 40% by rigidifying the surface ligands with bulky molecules. Bürgi et al. systematically studied the chirality and circular dichroism of Au_n(SR)_m and doped NCs. Very recently, Zhou et al. found an astonishing 3 orders of magnitude variation in carrier lifetime by tailoring the crystal phase of gold nanoclusters, indicating the critical role of atom packing in dictating the exciton lifetime and insight into the nonscalability.

All these advances are of great help with the understanding of the optical properties of gold NCs. Nevertheless, several important questions still remain unknown. First, how do the optical absorption, carrier dynamics, and their evolution relate to size and structure? Second, what role does the structure play in the optical properties of gold NCs with different sizes from small to large? Third, is there any correlation among the bandgap (E_g , or HOMO–LUMO gap), carrier lifetime, and nanocluster structure? Answering these questions requires a full size-series of gold NCs, and a grand view of the optical

properties is critically important for understanding the nonmetallic and metallic behaviors and further tailoring of the optical properties of metal NCs.⁵⁰ The intense research in recent years has accumulated a full series of nanocluster sizes, which motivated our current study.

Here, we discuss the grand evolution from nonscalable to scalable optical properties, including the bandgap (i.e., HOMO-LUMO gap in the quantized conduction band), optical absorption, transient absorption, and carrier dynamics of gold NCs ranging from tens to hundreds of gold atoms. By comparing their optical properties and correlating them with size/structure, we categorize the $Au_n(SR)_m$ NCs into three groups: (i) ultrasmall gold NCs (ca. <50 gold atoms), which show optical properties that are highly dependent on the structures so that they are nonscalable; (ii) medium-sized NCs (50-100 gold atoms), which exhibit both size and structuredependent optical properties so that they are in the transition regime from nonscalable to scalable; (iii) large-sized NCs (ca. >100 gold atoms), which show optical properties being only dependent on size while the structure effect disappears, and thus exhibit scalable optical properties. Building on the results, we also put forth some criteria for determining the metallic state of gold nanoclusters. Overall, this work reveals a grand "map" for the evolution of gold NCs from the quantumconfined state in ultrasmall sizes (<2 nm) to the metallic/ plasmonic state (at 2.2 nm) and serves as a paradigm for future research on other types of metal nanoclusters.

2. RESULTS AND DISCUSSION

2.1. Nonscalable Optical Properties of Small Gold NCs. It is worth mentioning that plasmonic Au or Ag NPs follow uniform scaling laws, such as the nearly linear relationship of SPR peak wavelengths vs dimensions (diameter for nanospheres⁵¹ or aspect ratio for nanorods⁵² and nanoprisms²). When the particle size is shrunk to the quantum-size regime, whether or not there is any universal scaling law remained elusive in the literature.

When the size of gold NCs approaches the de Broglie wavelength of Fermi electrons, $\lambda = h/m_e v \sim 0.52$ nm (where h is the Planck constant, m_e is the electron mass, and its velocity (v) is taken as 1.39 \times 10⁶ m/s), significant quantum confinement effects occur, which give rise to discrete electronic structure and multiple excitonic peaks. Figure 1A shows the UV-vis absorption spectra of Au₂₃(SR)₁₆, Au₂₄(SR)₂₀, $Au_{25}(SR)_{18}$, $Au_{28}(SR)_{20}$, $Au_{36}(SR)_{24}$, $Au_{38}(SR)_{24}$, $Au_{44}(SR)_{28}$, and $Au_{52}(SR)_{32}$ $(Au_{23}$, Au_{24} , Au_{25} , Au_{28} , Au_{36} , Au_{38} , Au_{44} , and Au₅₂ for short) NCs. Multiple absorption peaks are observed in all these gold NCs. The E_g of NCs in this size range can be easily obtained by extrapolating the absorbance to zero. As the size increases, the position of the lowest absorption peak, and, thus, the E_g , exhibits a zigzag trend. For example, from Au_{23} to Au_{24} , an addition of one gold atom gives rise to an E_g increase from 1.9 to 2.07 eV, instead of an expected reduction with increasing size. From Au_{24} to Au_{25} , $E_{\rm g}$ largely drops from 2.07 to 1.3 eV with the addition of one gold atom, instead of being scalable with the well-known $1/R^2$ law (R = radius) dictated by quantum confinement.⁵³ From Au₂₅ to Au₂₈, the E_g again increases from 1.3 to 1.77 eV as opposed to the expected drop. One can observe that the structure, rather than size, plays a dominant role in the $E_{\rm g}$ and optical property evolution in these ultrasmall NCs. From the UV-vis absorption, Au_{25} and Au_{38} NCs, which possess icosahedral cores, ^{15,54} exhibit relatively small E_g values. On the other hand, Au_{23} and Au_{24} , with a

cuboctahedral Au_{13} and a bitetrahedral Au_8 metal core, ^{55,56} respectively, show larger $E_{\rm g}$ values. As reported previously, the face-centered cubic (fcc) series (Au_{28} , Au_{36} , Au_{44} , Au_{52}) exhibits a uniform evolution in optical absorption and the $E_{\rm g}$ decreases slowly as the size increases. ^{57,58} This is because the effect of structure has been eliminated since they all share the same type of structure and a uniform growth pattern.

After comparing the UV-vis absorption spectra of these small gold NCs, here we further study their photodynamics by comparing their time-resolved transient absorption spectra in Figure 1B. Transient absorption (TA) measures the difference between the absorption of the excited state and that of the ground state (i.e., $\bar{\Delta}A$). The positive signal in ΔA represents excited-state absorption (ESA) whereas the negative signal stands for ground-state bleaching (GSB). We chose the TA spectra probed at 10 ps so that the hot carriers have cooled down. One can observe that these gold NCs show broad ESA spanning all over the visible range (400-800 nm) overlapped with GSB peaks (i.e., dips on the positive signal). The broad ESA, which is commonly observed in all sizes, suggests that these gold NCs have very dense excited states; this is different from the small organic molecules. Those lowest-energy GSB peaks are marked with arrows, and it is found that they exhibit a trend similar to that of the steady-state UV-vis absorption. It is also found that the profiles of the TA spectra are very different from one size to another, indicating drastically different electronic structures among these different sizes. This feature is consistent with the nonscalable feature of this size regime.

We now further compare their carrier lifetimes from the transient absorption measurements (Figure 1C). Since these small NCs show relatively long carrier lifetimes (>10 ns), a nanosecond probe (white continuum) was used in measurements. It is found that, with similar excitation energy, the hot carrier lifetime of these NCs generally increases as $E_{\rm g}$ decreases (see Figure S1A,B in Supporting Information). On the other hand, their band-edge carrier lifetimes exhibit an interesting trend: Except Au₃₈, which exhibits a short lifetime of 4 ns, all other sizes show long carrier lifetimes ranging from 90 to 200 ns. The very short lifetime in Au₃₈ can be explained by its very small E_{σ} (0.9 eV) (see Figure S2A,B). For all other sizes, the carrier lifetime only shows very subtle differences, which indicates that the size does not play an important role in the carrier lifetimes of these ultrasmall gold NCs. Very recently, we reported that the hexagonal close-packed (hcp) Au₃₀(SR)₁₈ nanocluster showed a very short carrier lifetime of 1 ns while the body-centered cubic (bcc) Au₃₈S₂(SR)₂₀ with comparable $E_{\rm g}$ showed a very long carrier lifetime of 4.7 μ s.⁵ Such an observation further indicates the importance of structure in small gold NCs. It is worth noting that altering the surface ligand's carbon tail may change the carrier lifetime to some extent; 59 however, the structure of the metal core plays a dominant role in carrier lifetime because the strong quantum confinement effect occurs in the metal core. Therefore, under similar experimental conditions (the same solvent, concentration, and pump power), the carrier lifetimes of these NCs are essentially dependent on their structures.

On the basis of the UV-vis absorption, TA spectra, and carrier lifetimes of these small NCs, it is concluded that these small NCs show nonscalable electronic and optical properties. Their properties are largely dependent on the structures (Figure 1D). Tailoring the core structure and composition of the metal core as well as the core-shell interaction will help to

broaden their optical applications, including photoluminescence, lasing, two-photon absorption, and solar energy harvesting.

2.2. Optical Properties of Medium-Sized Gold NCs. As the size increases, quantum confinement will become weaker, thus giving rise to smaller bandgaps and less pronounced absorption peaks due to crowdedness of electronic states. To resolve their optical gaps, absorption spectra in the NIR region will be needed. Here, three sizes are available, $\mathrm{Au_{64}(SR)_{32}}$, $\mathrm{Au_{92}(SR)_{44}}$, and $\mathrm{Au_{99}(SR)_{42}^{60-62}}$ ($\mathrm{Au_{64}}$, $\mathrm{Au_{92}}$, and $\mathrm{Au_{99}}$ for short), for comparing their optical properties and for mapping out the trend of optical properties in the medium size range. Among these three NCs, only the structure of $\mathrm{Au_{92}}$ has been solved and it shows an fcc metal core.

Figure 2A,B shows the UV-vis-NIR (300-3300 nm) absorption spectra on wavelength and energy scales,

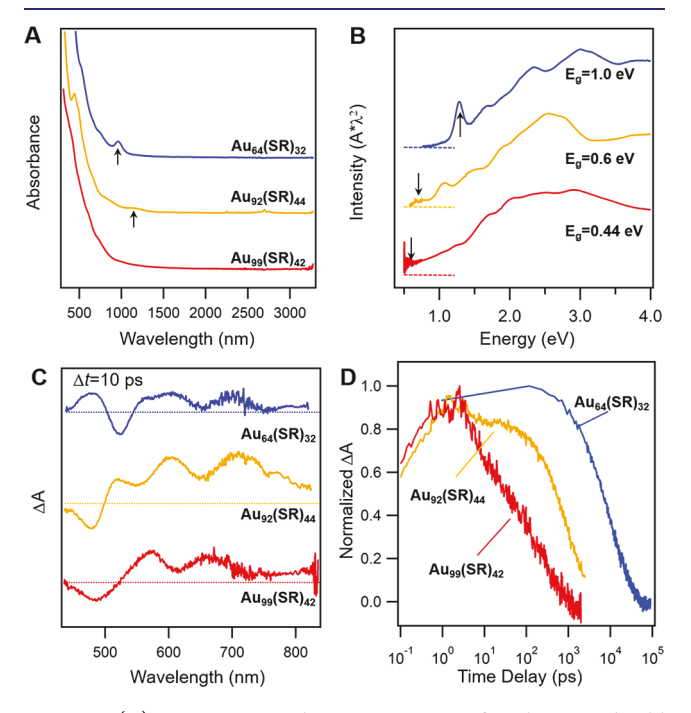


Figure 2. (A) UV–vis–NIR absorption spectra of medium-sized gold NCs. The lowest absorption peaks are marked with arrows (solvent: CCl_4). (B) Absorption spectra in energy scale. (C) Transient absorption spectra probed at 10 ps with 360 nm excitation. (D) Kinetic decays obtained from femtosecond and nanosecond time-resolved transient absorption spectroscopy.

respectively. The lowest absorption peak in Au₆₄ is measured to be at \sim 1000 nm (1.2 eV), and by extrapolating the peak to zero absorbance the $E_{\rm g}$ is estimated to be 1.0 eV. As the size increases to Au₉₂, one can observe that, in addition to the absorption peak at 1150 nm (1.08 eV), there is another shoulder at ~ 0.7 eV (Figure 2B). Therefore, the E_{σ} of Au₉₂ is estimated to be ~0.6 eV, which is comparable to the value of 0.49 eV measured by differential pulse voltammetry (DPV).⁶³ Interestingly, Au₉₂ exhibits a sharp absorption peak around 440 nm, which seems to be a typical feature of the fcc series. 57 Such a feature indicates that structure can still play an important role in the optical properties of gold NCs as large as Au₉₂. When the size further increases to Au₉₉, one can hardly observe any sharp absorption peaks and the spectrum starts to show only broad bands or humps. The $E_{\rm g}$ of Au₉₉ is estimated to be \sim 0.44 eV on the basis of the optical absorption (see Figure S3A,B for

details), which is similar to the value measured by DPV (0.4 eV). 64 Overall, from Au₆₄ to Au₉₉, one can see that $E_{\rm g}$ drastically decreases from 1 to 0.44 eV, which offers a good series to study the photodynamics versus bandgap of gold NCs.

The TA spectra of all three NCs are quite congested, consisting of broad ESA overlapped with several GSB peaks (Figure 2C). One can observe that TA spectra of Au₆₄ show a strong GSB at 525 nm and two weak GSBs at 650 and 750 nm (Figure 2C), which agrees with the steady-state absorption spectrum (Figure 2A). Similarly, in the TA spectra of Au₉₂ and Augg, one can observe three and four GSB peaks, respectively, overlapped with the broad ESA band in the visible range. Within the first 5-10 ps, the ESA peaks for all three NCs exhibit a fast decay, which should be explained as the hot carrier cooling to the band edge (see Figure S4A-D and Table S1 in Supporting Information for details). In the following 1– 100 ns, the electron-hole recombination occurs and the TA signal decays to zero. The carrier lifetimes of Au₆₄, Au₉₂, and Au₉₉ are determined to be 11.5 ns (Figures S5A,B and S6A), 1 ns (Figure S6B), and 700 ps (Figure S6C and Figure 7A-D), respectively. These are much shorter than the $\sim 10^2$ ns lifetimes of smaller NCs (n < ca. 50).

From both the evolution in $E_{\rm g}$ (Figure 2B) and carrier dynamics (Figure 2D), one can observe that the size starts to play an important role in the optical properties of medium-sized gold NCs, which is in contrast to the previously discussed ultrasmall sizes. Meanwhile, the spectral features of medium-sized gold NCs are still largely dependent on their structures. Therefore, in the medium size range $(Au_{64}-Au_{99})$, both structure and size determine the optical properties of gold NCs.

2.3. Optical Properties of Large-Sized Gold NCs. When the gold NCs contain more than ca. 100 Au atoms, their UV-vis spectra typically show broad and weak absorption bands. Moreover, it is almost impossible to resolve their optical bandgaps since the E_g is smaller than 0.4 eV, i.e., extending into the IR region, where absorptions by solvent and surface functional groups dominate. Their E_g values can only be determined by electrochemical DPV measurements. 66 Here, we compare the optical properties of Au₁₀₃S₂(SR)₄₁, ${\rm Au_{130}(SR)_{50}}, {\rm Au_{133}(SR)_{52}}, {\rm Au_{144}(SR)_{60}}, {\rm and} {\rm Au_{246}(SR)_{80}} \\ {\rm (Au_{103}, Au_{130}, Au_{133}, Au_{144}, Au_{246} \ for \ short)}.^{24,25,63-67} {\rm The}$ crystal structures of all of these five NCs have been solved. As shown in Figure 3A, Au₁₀₃ possesses a Marks decahedron Au₇₉ kernel, 65 and Au₁₃₀ shows an Au₁₀₅ decahedron core. 66 Au₁₃₃ and Au₁₄₄ have icosahedral Au₁₀₇ and Au₁₁₄ cores, ²⁴, respectively, and Au_{246} shows a metal core composed of an Ino decahedron Au₁₁₆ plus a Au₉₀ shell.⁶⁷ Interestingly, the smaller four NCs exhibit relatively weak and broad absorption peaks, while Au₂₄₆ exhibits a prominent absorption peak at 460 nm (Figure 3B). It is also worth noting that all four smaller NCs (Au₁₀₃, Au₁₃₀, Au₁₃₃, Au₁₄₄) show very similar UV-vis absorption profiles.

The transient absorption spectra of these large NCs are compared in Figure 3C. Surprisingly, the TA spectra of Au₁₀₃, Au₁₃₀, Au₁₃₃, and Au₁₄₄ show very similar profiles, which agree with their UV—vis absorption. If we further compare the TA spectra of these four NCs with that of Au₉₉, it is found that they all share some common features (Figure S8A—D): (1) Three major GSB peaks in the visible range (400—800 nm), and (2) both ESA and GSB peak intensities are rather low (less than 2 milli-OD). It is known that the steady-state and

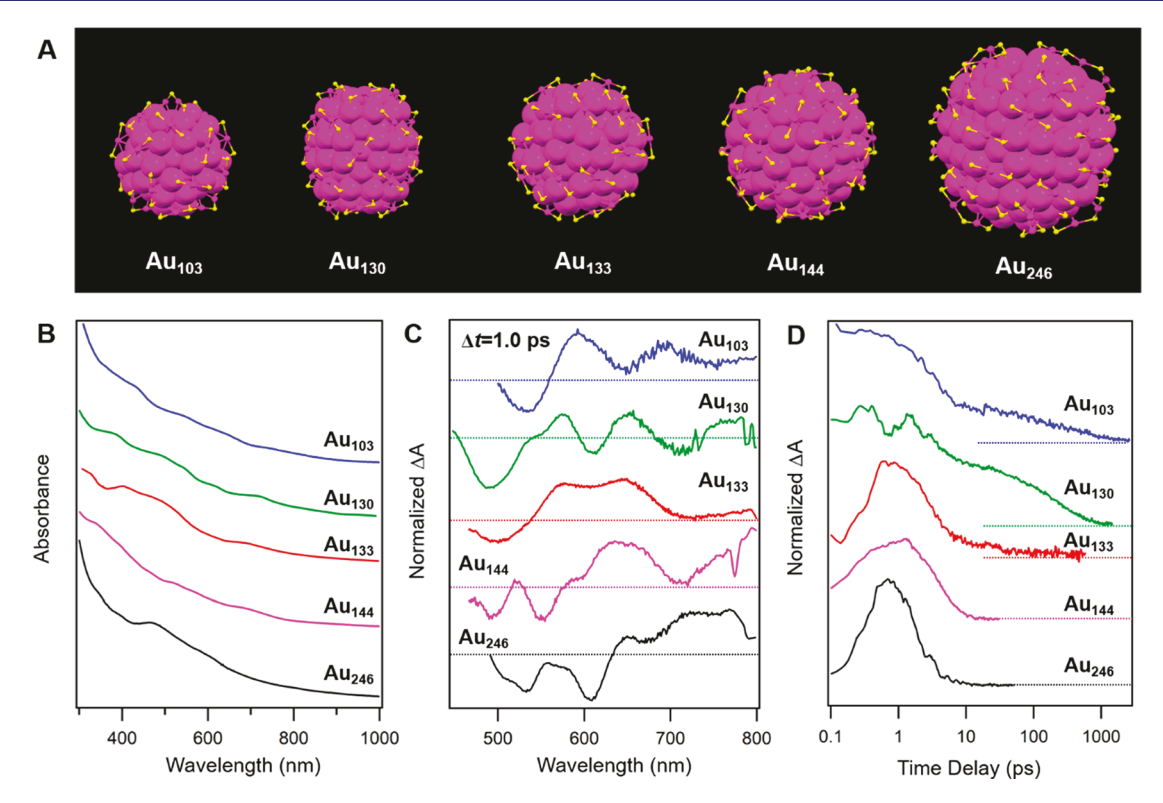


Figure 3. (A) Crystal structures of Au_{103} , Au_{130} , Au_{130} , Au_{130} , Au_{144} , and Au_{246} NCs (color labels: magenta = Au, yellow = S, carbon tails are omitted for clarity). (B) UV—vis absorption spectra of all five gold NCs. (C) Transient absorption spectra of the five NCs at time delay 1 ps. (D) Kinetic decays probed at selected wavelengths.

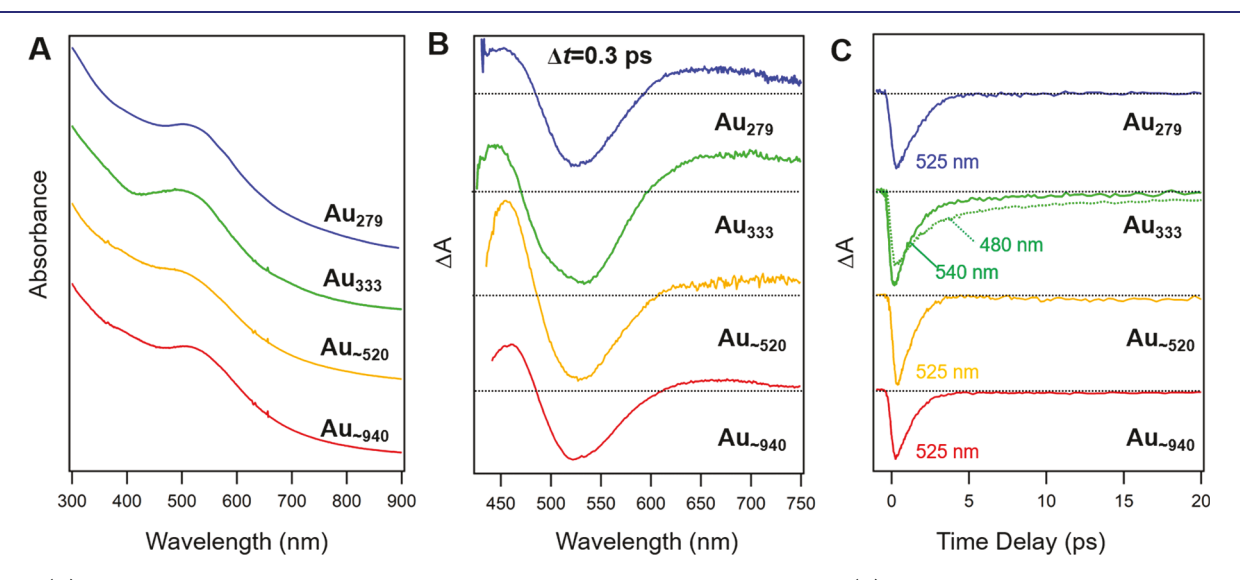


Figure 4. (A) UV-vis absorption spectra of a series of atomically precise, plasmonic Au NPs. (B) Transient absorption spectra of these NPs probed at 0.3 ps. (C) Kinetic traces probe at the maximum of the SPR of all gold NPs.

transient absorption spectra of small-sized gold NCs are closely related to their structures. Here, similar TA spectra indicate that although they possess different numbers of gold atoms in the core and different structures, their electronic structures are indeed similar. Such an observation indicates that the structure effect fades out in these large gold NCs and the size solely dominates and plays the decisive role in their optical properties.

After looking into the relaxation dynamics of these five NCs, one can find that the decay becomes faster as the size increases (Figure 3D). From Au_{103} to Au_{246} , the decay lifetime drops

from 400 to 2 ps. 21,24,65,68,69 Moreover, the relaxation pathway also experiences distinct evolution as the size increases. In Au₁₃₀, one can observe an additional fast decay (\sim 1 ps) with 360 nm (3.4 eV) excitation, which is absent when pumped at 1200 nm (\sim 1 eV). 68 This fast relaxation should be explained as internal conversion or hot carrier cooling, which occur over a very short time. In Au₁₃₃ and Au₁₄₄, on the other hand, the fast relaxation is absent even with UV excitation. Moreover, the decay time constants are independent of the excitation energy. We have tested the power dependence on all of these five gold NCs, and their TA decays are found to be independent of the

Journal of the American Chemical Society

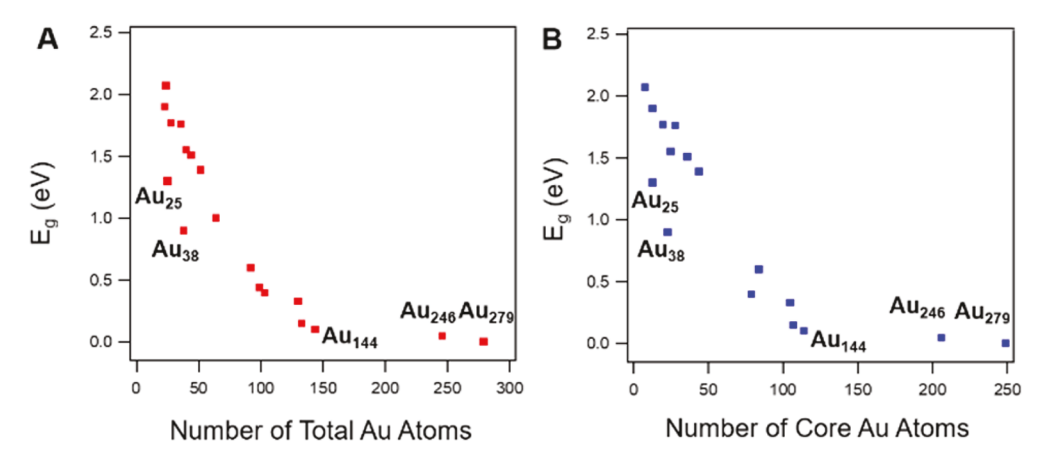


Figure 5. (A) Bandgap as a function of number of total Au atoms. (B) Bandgap as a function of core Au atoms.

pump fluence. 21,24,65,68,69 In contrast to plasmonic gold NPs, the power-independent dynamics suggests that all these NCs are still in the molecular state.

On the basis of the results discussed above, we can conclude that gold NCs larger than ca. 100 atoms can be viewed as entering the scalable size regime, in which the structure plays a less important role in their optical properties and the size instead becomes the sole dominant factor determining their absorption and electron dynamics. Of note, the giant Au₂₄₆ (2.2 nm metal core diameter) is the largest nonmetallic gold nanocluster reported so far.

2.4. Optical Properties of Giant Gold NCs with Nascent SPR. Recently, we reported that, with addition of merely 33 gold atoms, i.e., from Au₂₄₆ to Au₂₇₉, a sharp transition from a nonmetallic to a metallic state occurs. 69,70 Such a sharp transition is not only reflected in UV-vis absorption spectra, but also in the transient spectra and electron dynamics. For those sizes $\geq Au_{279}$ (including Au_{279}) Au_{333} , $Au_{\sim 520}$, $Au_{\sim 940}$), $a_{\sim 520}$, $a_{\sim 940}$, $a_{\sim 940}$), $a_{\sim 940}$, one can observe an SPR peak in the UV-vis absorption spectra (Figure 4A). These SPR peaks are less prominent due to smaller sizes (2.2-3 nm) compared to conventional NPs with SPR (>5 nm). The weaker SPR in these thiolate-protected Au, NCs or NPs can also be ascribed to chemical damping⁵¹ as well as the thiolate ligands that give rise to scattering of electrons across the inorganic/organic interface. The is worth noting that the SPR peak becomes more significant in Au₃₃₃ and then weak again in Au_{~520} and Au_{~940}. Such an observation indicates that Au₃₃₃ is special among these four nanoparticles.

When one examines the transient absorption spectra of these Au, NPs, one can observe very similar features: a broad negative GSB due to the SPR and two ESA wings on the two sides of the GSB (Figure 4B). Such a spectral profile is a typical observation in plasmonic gold NPs. In contrast to the case of smaller, nonmetallic gold NCs, there is no bandgap in these plasmonic Au, NPs. A femtosecond laser will heat the electrons in these Au_n particles to a very high temperature.⁷² Following the electron-phonon coupling process, the Au⁺ lattice will expand, and the SPR will broaden. Therefore, the bandwidth of the GSB due to SPR is also dependent on the electron temperature. Here, we compare the TA spectra at low pump fluence ($<3 \mu J/cm^2$) so that the pump laser will not lead to broadening of the SPR. One can see that the evolution of GSB in TA is similar to that in UV-vis absorption: in Au₂₇₉₁ $Au_{\sim 520}$, and $Au_{\sim 940}$ their GSB is uniformly located at 525 nm,

while in Au₃₃₃, two GSB bands at 480 and 540 nm can be observed.

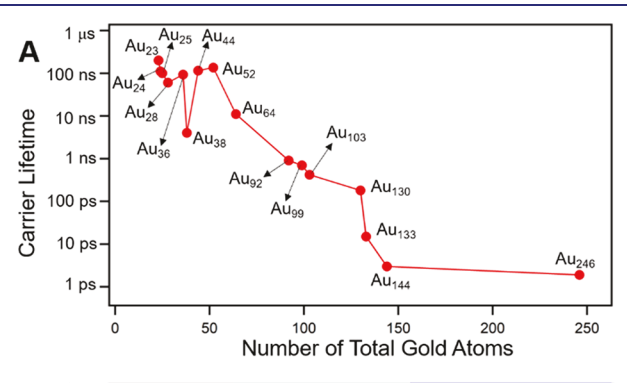
The electron dynamics in plasmonic gold NPs can be explained by a two-temperature model. As the electrons are heated up by the laser, heat will flow from electrons to the lattice via electron-phonon coupling (e-p for short); then, the energy will further dissipate into the environment through phonon-phonon coupling (ph-ph). The e-p process is dependent on the initial electronic temperature and thus dependent on pump fluences. Typically, e-p coupling occurs between 1 and 5 ps, dependent on the pump fluences. Figure 4C shows the kinetic decays probed at GSB maxima in these Au_n NPs with very low pump fluences ($<3 \mu J/cm^2$). In Au₂₇₉, Au_{~520}, and Au_{~940}, we compared the kinetic decays probed at 525 nm. In Au₃₃₃, on the other hand, we plot the decays probed at 540 and 480 nm. The TA dynamics in all Au, NPs experience a fast decay within 5 ps, followed by a slow decay (>10 ps). In Au₃₃₃, the TA decay probed at 540 nm is similar to that of other sizes while the TA decay probed at 480 nm shows a relatively slower decay. Such an observation again indicates that Au₃₃₃ is peculiar among these four Au_n NPs, which was explained as the anisotropic shape. 73 The fast decay components in all four NCs are around 1 ps, which should be explained as e-p coupling. Our recent study has shown that the e-p coupling time increases as the size increases. 21 Such an observation further indicates that the size plays a major role in the optical properties of these plasmonic NPs, which are hence scalable in this size regime. It is worth noting that, in plasmonic gold NPs, surface ligands could also change the optical absorption by changing the screening effect via withdrawing or donating electrons.⁷¹ Therefore, changing ligands in plasmonic gold NPs may also modulate their optical properties including absorption and electron dynamics.

2.5. Bandgap Evolution in All Sizes of Thiolate-**Protected Gold NCs.** After showing the optical properties versus size in $Au_n(SR)_m$, we then sort out the rules behind these observations. First, we discuss the bandgap versus size. Figure 5A plots the E_g versus the number of gold atoms in the NCs. It can be seen that the $E_{\rm g}$ generally shrinks as the size increases, but the evolution is not smooth. The Au₂₅, Au₃₈, Au₁₃₃, and Au₁₄₄ samples exhibit much smaller bandgaps compared to those with similar sizes; this is owing to the nature of their icosahedral structures in which valence electron wave functions are more extensive (i.e., over the entire core without local segregation). For all other sizes, E_{σ} is inversely proportional to the total number of gold atoms. Furthermore, there is a turning point at $n \sim 100$; it is found that the slope becomes smaller for those sizes larger than ca. 100 atoms.

If one further plots the $E_{\rm g}$ as a function of the number of gold atoms in the core (Figure 5B), one can find that Au₂₅, Au_{38} , Au_{133} , and Au_{144} still exhibit much smaller E_g values compared to similar sizes. The evolution trend is similar to that in Figure 5A, and a good linearity can be found between E_g and the number of core gold atoms. There is also a turning point at the Au₁₀₃ NC (note: it has 79 gold atoms in the core); those larger than Au_{103} show slower shrinking of E_g as the size increases. The turning point at ~100 gold atoms in both cases is also coincident with the transition in their optical properties discussed in Section 2.3, where all those NCs larger than Au₉₉ show similar UV-vis absorption and TA spectra.

The similar trend in E_g versus the total gold atoms or the core gold atoms indicates that the $E_{\rm g}$ is largely determined by the size of the metal core. Meanwhile, a relatively smaller $E_{\rm g}$ value in the icosahedral series (Au₂₅, Au₃₈, Au₁₃₃, and Au₁₄₄) suggests that the atomic structure can also affect the E_g by modulating the electronic structure in gold NCs.

2.6. Energy Gap Rule. Given all the time-resolved experimental results, we are now able to picture the grand evolution of carrier lifetime versus the size and bandgap of $Au_n(SR)_m$ as shown in Figure 6A,B. It is worth noting that all



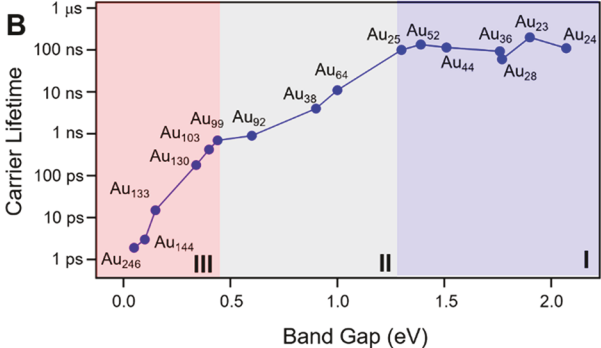


Figure 6. (A) Carrier lifetime versus the total number of gold atoms and (B) carrier lifetime versus bandgap for thiolate-protected gold NCs reported so far.

the TA measurements are performed in dilute toluene solutions to rule out the effect of environment. Figure 6A shows the carrier lifetime versus the total number of gold atoms. One can observe that all those small sizes (<ca. 50 atoms) show similar carrier lifetimes (on the order of 10² ns) except for Au₃₈ (4 ns) which has a small E_g (0.9 eV). As the size increases, carrier lifetime starts to decrease, and there is a drastic decrease in lifetime starting from Au₁₃₀. When the size further increases from Au₁₄₄ to Au₂₄₆, the carrier lifetime

remains the same (2-3 ps). After we further plot the carrier lifetime versus $E_{g'}$ a stronger correlation can be observed in Figure 6B. On the basis of their carrier lifetimes and bandgaps, gold NCs can be clearly divided into three groups.

- Group I: For those with $E_g > \text{ca. } 1.3 \text{ eV}$ (size n < ca. 50), their optical properties are strongly dependent on the structure, and interestingly, their carrier lifetimes are relatively insensitive to the bandgap (except the hcp Au₃₀ and bcc Au₃₈, 5 not drawn here). One can observe that Au₂₃, Au₂₄, Au₂₅, and the fcc series (Au₂₈, Au₃₆, Au₄₄ and Au₅₂) have similar carrier lifetimes of ~100 ns despite the change in E_g from 1.3 to 2.07 eV.
- Group II: For NCs with E_g between 0.44 and 1.3 eV, their carrier lifetimes start to show a distinct dependence on $E_{\rm g}$, and the lifetime varies between ~100 and ~1 ns.
- \bullet Group III: For NCs with $E_{\rm g}$ < 0.44 eV, the carrier lifetime is more sensitive to $E_{\rm g}$ and accelerates rapidly from 700 to 1.5 ps.

Unraveling such a grand evolution is very helpful for understanding the optical properties of gold NCs. For those gold NCs in group I, the structure plays a significant role in their optical properties and E_g plays a less important role in carrier lifetimes. By tailoring the core and surface structure, it is feasible to change their absorption, photoluminescence, and other optical properties. For those in group II, the structure still determines the optical absorption, but the carrier lifetime starts to show a dependence on $E_{\rm g}$. In group III, the $E_{\rm g}$ of NCs is smaller than 0.4 eV; the structure plays a less prominent role in their optical absorption, and the carrier recombination rate is limited by $E_{\rm g}$. It is also interesting to see that although those NCs in group II and group III are protected by different thiolate ligands (i.e., different R groups), the carrier lifetimes follow well the energy gap law, which indicates that surface ligands (R groups) play a less important role in the carrier dynamics.

According to the energy gap law, the nonradiative recombination rate $k_{\rm nr}$ can be expressed as a function of $E_{
m g}$ as follows:74

$$k_{\rm nr} = A e^{-\gamma E_g/\hbar\omega}$$

Here, γ describes the molecular parameters, and ω is the highest vibration frequency involved in the nonradiative decay. It is known that most of the gold NCs show very low photoluminescence quantum yields (QY < 1%) so that the carrier recombination is dominated by nonradiative decay. Thus, the recombination rate measured by TA can be estimated as $k_{\rm nr}$ here. After we plot $\ln k_{\rm nr}$ as a function of $E_{\rm g}$ (Figure 7), one can observe that $k_{\rm nr}$ and $E_{\rm g}$ show a good linear relationship for those with $E_{\rm g}$ less than 1.3 eV, and there is a turning point at 0.44 eV, which agrees well with the trend in Figure 5A,B. The linear fitting gives two gradients of -5.5 eV^{-1} and $-15.1~{\rm eV}^{-1}$ for the regime 0.44 eV < $E_{\rm g}$ < 1.3 eV and for $E_{\rm g}$ < 0.44 eV, respectively. It is known that γ/ω would determine the nonradiative decay and a higher vibrational frequency would give rise to faster nonradiative decay. Here, we find an increase in the nonradiative decay for those larger than Au₉₉, which indicates that there should be a decrease in γ / ω value for those NCs with $E_{\rm g}$ < 0.44 eV.

All those NCs with E_g larger than 1.3 eV show similar carrier lifetimes. Such an observation indicates that the lifetimes of these NCs are limited for some reason. A closer look at these NCs indicates that they all share a metal core containing

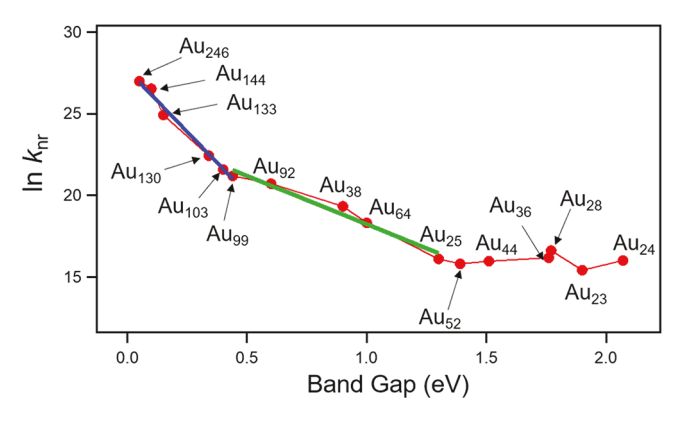


Figure 7. Plot of $\ln k_{nr}$ versus E_g for thiolate-protected gold NCs (solid lines are best linear fits for the data).

segregated Au₄-tetrahedron units (Au₂₃, Au₂₄, Au₂₈, Au₃₆, Au₄₄, Au₅₂). The tetrahedron units are closely coupled to each other so that energy will be dissipated to neighboring tetrahedron units efficiently, leading to limited carrier lifetimes (100-200 ns). The feature of segregation of tetrahedral Au_4 fades out in larger sizes, cf., Au_{52} and Au_{92} . This explains the 1.3 eV turning point seen at the transition from nonscalable to scalable optical properties in gold NCs as discussed above. Thus, the 1.3 eV turning point primarily reflects the structural influence.

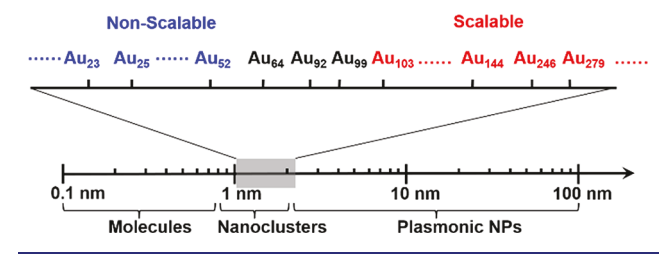
As for those NCs with E_g < 0.44 eV, the carrier lifetimes decrease faster with size than those of smaller sizes. This could be explained by the stronger electron-phonon coupling in larger sizes. For the latter, it is found that all these large-sized gold NCs exhibit strong oscillations in their TA dynamics (Figures S9A-F and S10A-F), which can be explained by the coherent phonons. 69,75-77 The coupling between phonon and carrier recombination becomes larger as the size increases. Especially in Au₂₄₆, the carrier lifetime is very close to the lifetime of coherent phonons, 69 indicating very strong coupling. Such a strong coupling can explain the decreases in γ/ω of those with $E_{\rm g}$ < 0.44 eV. Furthermore, the stronger coupling between the vibrations of surface ligands (carbon tails) and the metal core relaxation could also explain the fast recombination observed in large-sized gold NCs. 42,43 Taken together, the electron-phonon coupling and the core energy dissipation through ligand vibrations explain the ~0.4 eV turning point and the more rapid drop in lifetime for group III than group II.

The structure effect on carrier lifetimes can be clearly observed in group I NCs. All those NCs containing Au₄tetrahedron units (Au $_{23}$, Au $_{24}$, Au $_{28}$, Au $_{36}$, Au $_{44}$, Au $_{52}$) show a relatively large $E_{\rm g}$ compared with other structures of similar sizes; thus, a uniform evolution can be observed (Figure 5A). However, their carrier lifetimes are limited to ∼100 ns (Figure 6B) regardless of E_g , which is explained as efficient energy transfer between neighboring Au₄ units. On the other hand, icosahedral Au₂₅ and Au₃₈ nanoclusters show relatively smaller E_g values compared to other similar sizes (1.3 eV for Au₂₅ and 0.9 eV for Au₃₈) as a result of more extensive valence electron wave functions (see Section 2.5). Therefore, the carrier lifetime decreases drastically from 100 ns for Au₂₅ to 4 ns for Au₃₈. For group II and III NCs ($E_{\rm g}$ < 1.3 eV), there is less structural effect on carrier lifetimes (Figure 7), and $E_{\rm g}$ plays a more important role in determining the excited-state relaxation.

2.7. From Nonscalable to Scalable Optical Properties.

According to all the above results and discussions, we can summarize the grand evolution from nonscalable to scalable optical properties in $Au_n(SR)_m$. On the basis of the UV-vis-NIR absorption, transient absorption spectra, and carrier lifetimes, gold NCs can be categorized into three groups (Scheme 1):

Scheme 1. Summary of Evolution from Nonscalable to Scalable Optical Properties in Thiolate-Protected Gold NCs



- (1) Nonscalable NCs (small sizes, ca. ≤50 atoms): For those ultrasmall NCs smaller than Au52, the structure rather than size determines the optical bandgap, UV-vis absorption, and TA spectra, as well as carrier dynamics. The optical properties of these ultrasmall NCs are thus nonscalable.
- (2) Medium-sized NCs: Gold NCs in the medium size range (Au₆₄, Au₉₂, Au₉₉) show optical properties dependent on both size and structure. The optical bandgap and carrier lifetimes are significantly dependent on size, while the UV-vis absorption spectra are still largely determined by their atomic structures.
- (3) Scalable NCs (large sizes, ca. ≥100 atoms): For those NCs larger than Au₉₉, the effect of structure on optical properties fades out and the optical properties show a uniform size dependence regardless of the structure types. Especially, the UV-vis absorption as well as TA spectra are similar for those larger than Au₉₉, and the lifetime also decreases smoothly as the size increases. Furthermore, those NCs larger than Au₂₇₉ all show an SPR peak and plasmonic optical properties. Therefore, the optical properties of these giant NCs are scalable.

2.8. Criteria for Determining the Metallic State of Au **NCs.** Since large Au NCs will become metallic Au NPs as the size increases, it is important to understand and probe the features of metallicity. On the basis of the studies on gold NCs, we summarize the following criteria, which may provide guiding principles for future studies on other metal NCs (e.g., Ag) and alloyed ones.

- (1) Steady-state and transient absorption spectra: In the UV-vis absorption spectra, molecular-like Au NCs show multiple absorption peaks while metallic Au NPs exhibit a single SPR peak (for spherical ones). Moreover, from the UV-vis-NIR absorption spectra, it is possible to estimate the optical bandgap of molecular-like Au NCs if the gap is not too small ($E_{\rm g} > 0.4$ eV), while metallic AuNPs show zero bandgap. Similarly, Au NCs show multiple GSB peaks in their TA spectra while Au NPs show single GSBs corresponding to SPR (for spherical
- (2) Cryogenic spectra: The absorption spectra of molecularlike Au NCs will be sharpened, intensified, and blue-

- shifted as the temperature decreases,³⁷ while those of metallic plasmonic Au NPs are less affected by the surrounding temperature.⁷⁰
- (3) Excited-state lifetime: As discussed in Section 2.6, the excited-state lifetime of Au NCs is dependent on $E_{\rm g}$ so that it varies from several picoseconds to microseconds. On the other hand, the electron dynamics of metallic gold NPs show rapid e-p coupling (about 1 ps) followed by a ~ 100 ps ph-ph coupling, which is less dependent on their size.
- (4) Power dependence: Molecular-like Au NCs show power-independent electron dynamics, while metallic Au NPs show observable power dependence in their dynamics. As the size of Au NPs increases, the power dependence becomes more significant and prominent.
- (5) Coherent phonons: Both Au NCs and NPs show coherent oscillations in TA dynamics, which originate from coherent phonons. In Au NPs, the phonon frequency (ν) is inversely proportional to diameter (scaling law: $\nu \sim d^{-1}$). In Au NCs, phonon frequency is largely dependent on their structures.

3. CONCLUSION

In summary, we have systematically probed the three-stage evolution from nonscalable to scalable optical properties in thiolate-protected gold NCs, as well as the exciton to plasmon transition. By comparing the bandgap, UV-vis-NIR absorption spectra, transient absorption spectra, and carrier dynamics, we conclude that $Au_n(SR)_m$ NCs can be categorized into three stages: nonscalable sizes (n < ca. 50 atoms), medium sizes (\sim 50 to \sim 100), and scalable regime of large sizes (>ca. 100). In nonscalable NCs ($E_g = 2.1-1.3$ eV), all the optical properties are heavily influenced by the detailed atom packing structures. In medium-sized NCs ($E_g = 1.3-0.4$ eV), both size and structure determine the optical properties. In the scalable NCs ($E_g = 0.4-0$ eV), the structure effect essentially fades out and the size solely determines their optical properties. The first turning point of $n \sim 50$ and $E_{\rm g} \sim 1.3$ eV is largely due to the structural effect (i.e., predominant segregation of tetrahedral Au₄ in group I but fading out in larger sizes), whereas the second turning point of $n \sim 100$ and $E_g \sim 0.4$ eV is associated with stronger electron-phonon coupling as well as core energy dissipation via ligand vibrations in group III NCs. On the basis of the analyses, we also put forth some criteria for determining the nonmetallic and metallic states of gold NCs. The grand evolution of gold NCs in optical properties and the obtained principles will be of great importance to understand and predict the optical properties of other metal NCs as well as bimetal systems. The obtained insight will also provide guiding principles for developing the applications of metal NCs in photoluminescence, nonlinear optics, light harvesting, etc.

4. EXPERIMENTAL SECTION

- **4.1. Sample Preparations.** The syntheses of all gold NCs in this paper followed the methods reported previously. $^{15,21,24,25,54-57,60-62,65-67,70}$
- **4.2.** UV–Vis–NIR Absorption. The steady-state absorption spectra were measured at room temperature using a Shimadzu UV-3600+ spectrometer. For those absorption spectra measured between 300 and 1100 nm, toluene was used as the solvent. For those absorption spectra measured between 300 and 3300 nm, carbon tetrachloride (CCl₄) was used as the solvent.

4.3. Transient Absorption Spectra. The femtosecond TA spectroscopic measurements were performed on a commercial Ti:sapphire laser system (Spitfire Spectra Physics). The ~100 fs laser pulses in the ultraviolet and near-infrared regions of the spectrum were generated by a 3.5 mJ regenerative amplifier system (Spitfire, Spectra-Physics) and optical parametric amplifier (OPA, TOPAS). A small portion of the laser fundamental was focused into a sapphire plate to produce a supercontinuum both in the visible range, which overlapped with the pump in time and space. Multiwavelength transient spectra were recorded using dual spectrometers (signal and reference) equipped with array detectors whose data rates exceed the repetition rate of the laser (1 kHz). Dilute solutions of metal clusters in 1 mm path length cuvettes were excited by the tunable output of the OPA (pump). All the measurements were performed in toluene, and the optical density was adjusted to be about 0.3 OD at the excitation wavelength. Nanosecond transient absorption measurements were conducted using the same ultrafast pump pulses along with an electronically delayed supercontinuum light source with a subnanosecond pulse duration (EOS, Ultrafast Systems).

ASSOCIATED CONTENT

S Supporting Information

The Supporting Information is available free of charge at https://pubs.acs.org/doi/10.1021/jacs.9b09066.

Details of the transient absorption spectra and carrier dynamics of differently sized gold NCs, supporting Figures S1–S10, and supporting Table S1 (PDF)

AUTHOR INFORMATION

Corresponding Author

*rongchao@andrew.cmu.edu

ORCID 0

Meng Zhou: 0000-0001-5187-9084 Tatsuya Higaki: 0000-0002-6759-9009 Matthew Y. Sfeir: 0000-0001-5619-5722 Rongchao Jin: 0000-0002-2525-8345

Author Contributions

M.Z., T.H., and Y.L. contributed equally.

Notes

The authors declare no competing financial interest.

ACKNOWLEDGMENTS

R.J. acknowledges the financial support from the National Science Foundation (DMR-1808675).

■ REFERENCES

- (1) Hartland, G. V. Optical Studies of Dynamics in Noble Metal Nanostructures. *Chem. Rev.* **2011**, *111*, 3858–3887.
- (2) Jin, R.; Charles Cao, Y.; Hao, E.; Metraux, G. S.; Schatz, G. C.; Mirkin, C. A. Controlling Anisotropic Nanoparticle Growth through Plasmon Excitation. *Nature* **2003**, *425*, 487–490.
- (3) Mie, G. Beiträge zur Optik trüber Medien, speziell kolloidaler Metallösungen. *Ann. Phys. (Berlin, Ger.)* **1908**, 330, 377–445.
- (4) Song, Y.; Jin, S.; Kang, X.; Xiang, J.; Deng, H.; Yu, H.; Zhu, M. How a Single Electron Affects the Properties of the "Non-Superatom" Au₂₅ Nanoclusters. *Chem. Mater.* **2016**, *28*, 2609–2617.
- (S) Zhou, M.; Higaki, T.; Hu, G.; Sfeir, M. Y.; Chen, Y.; Jiang, D.-e.; Jin, R. Three-orders-of-magnitude Variation of Carrier Lifetimes with Crystal Phase of Gold Nanoclusters. *Science* **2019**, *364*, 279–282.
- (6) Yao, Q.; Chen, T.; Yuan, X.; Xie, J. Toward Total Synthesis of Thiolate-Protected Metal Nanoclusters. *Acc. Chem. Res.* **2018**, *51*, 1338–1348.

- (7) Wang, S.; Li, Q.; Kang, X.; Zhu, M. Customizing the Structure, Composition, and Properties of Alloy Nanoclusters by Metal Exchange. *Acc. Chem. Res.* **2018**, *51*, 2784–2792.
- (8) Gan, Z.; Xia, N.; Wu, Z. Discovery, Mechanism, and Application of Antigalvanic Reaction. *Acc. Chem. Res.* **2018**, *51*, 2774–2783.
- (9) Lei, Z.; Wan, X.-K.; Yuan, S.-F.; Guan, Z.-J.; Wang, Q.-M. Alkynyl Approach toward the Protection of Metal Nanoclusters. *Acc. Chem. Res.* **2018**, *51*, 2465–2474.
- (10) Kwak, K.; Lee, D. Electrochemistry of Atomically Precise Metal Nanoclusters. *Acc. Chem. Res.* **2019**, *52*, 12–22.
- (11) Ghosh, A.; Mohammed, O. F.; Bakr, O. M. Atomic-Level Doping of Metal Clusters. Acc. Chem. Res. 2018, 51, 3094-3103.
- (12) Ramakrishna, G.; Varnavski, O.; Kim, J.; Lee, D.; Goodson, T. Quantum-Sized Gold Clusters as Efficient Two-Photon Absorbers. *J. Am. Chem. Soc.* **2008**, *130*, 5032–5033.
- (13) Abbas, M. A.; Kamat, P. V.; Bang, J. H. Thiolated Gold Nanoclusters for Light Energy Conversion. *ACS Energy Lett.* **2018**, *3*, 840–854.
- (14) Russier-Antoine, I.; Bertorelle, F.; Calin, N.; Sanader, Z.; Krstic, M.; Comby-Zerbino, C.; Dugourd, P.; Brevet, P.-F.; Bonacic-Koutecky, V.; Antoine, R. Ligand-core NLO-phores: a Combined Experimental and Theoretical Approach to the Two-photon Absorption and Two-photon Excited Emission Properties of Small-ligated Silver Nanoclusters. *Nanoscale* **2017**, *9*, 1221–1228.
- (15) Zhu, M.; Aikens, C. M.; Hollander, F. J.; Schatz, G. C.; Jin, R. Correlating the Crystal Structure of A Thiol-Protected Au₂₅ Cluster and Optical Properties. *J. Am. Chem. Soc.* **2008**, *130*, 5883–5885.
- (16) Aikens, C. M. Electronic and Geometric Structure, Optical Properties, and Excited State Behavior in Atomically Precise Thiolate-Stabilized Noble Metal Nanoclusters. *Acc. Chem. Res.* **2018**, *51*, 3065–3073.
- (17) Jiang, D.-e.; Kühn, M.; Tang, Q.; Weigend, F. Superatomic Orbitals under Spin-Orbit Coupling. *J. Phys. Chem. Lett.* **2014**, 5, 3286–3289.
- (18) Yang, S.; Chen, S.; Xiong, L.; Liu, C.; Yu, H.; Wang, S.; Rosi, N. L.; Pei, Y.; Zhu, M. Total Structure Determination of $Au_{16}(S-Adm)_{12}$ and $Cd_1Au_{14}(S^tBu)_{12}$ and Implications for the Structure of $Au_{15}(SR)_{13}$. J. Am. Chem. Soc. **2018**, 140, 10988–10994.
- (19) Hossain, S.; Niihori, Y.; Nair, L. V.; Kumar, B.; Kurashige, W.; Negishi, Y. Alloy Clusters: Precise Synthesis and Mixing Effects. *Acc. Chem. Res.* **2018**, *51*, 3114–3124.
- (20) Kim, M.; Tang, Q.; Narendra Kumar, A. V.; Kwak, K.; Choi, W.; Jiang, D.-e.; Lee, D. Dopant-Dependent Electronic Structures Observed for $M_2Au_{36}(SC_6H_{13})_{24}$ Clusters (M = Pt, Pd). J. Phys. Chem. Lett. **2018**, 9, 982–989.
- (21) Zhou, M.; Zeng, C.; Chen, Y.; Zhao, S.; Sfeir, M. Y.; Zhu, M.; Jin, R. Evolution from the Plasmon to Exciton State in Ligand-protected Atomically Precise Gold Nanoparticles. *Nat. Commun.* **2016**, *7*, 13240.
- (22) Thanthirige, V. D.; Kim, M.; Choi, W.; Kwak, K.; Lee, D.; Ramakrishna, G. Temperature-Dependent Absorption and Ultrafast Exciton Relaxation Dynamics in MAu₂₄(SR)₁₈Clusters (M = Pt, Hg): Role of the Central Metal Atom. *J. Phys. Chem. C* **2016**, *120*, 23180–23188.
- (23) Zhou, M.; Yao, C.; Sfeir, M. Y.; Higaki, T.; Wu, Z.; Jin, R. Excited-State Behaviors of M₁Au₂₄(SR)₁₈ Nanoclusters: The Number of Valence Electrons Matters. *J. Phys. Chem. C* **2018**, *122*, 13435–13442.
- (24) Zeng, C.; Chen, Y.; Kirschbaum, K.; Appavoo, K.; Sfeir, M. Y.; Jin, R. Structural Patterns at All Scales in a Nonmetallic Chiral Au₁₃₃(SR)₅₂ Nanoparticle. *Sci. Adv.* **2015**, *1*, No. e1500045.
- (25) Yan, N.; Xia, N.; Liao, L.; Zhu, M.; Jin, F.; Jin, R.; Wu, Z. Unraveling the Long-pursued Au₁₄₄ Structure by X-ray Crystallography. *Sci. Adv.* **2018**, *4*, eaat7259.
- (26) Negishi, Y.; Nobusada, K.; Tsukuda, T. Glutathione-protected Gold Clusters Revisited: Bridging the Gap between Gold(I)-thiolate Complexes and Thiolate-protected Gold Nanocrystals. *J. Am. Chem. Soc.* 2005, 127, 5261–5270.

- (27) Negishi, Y.; Nakazaki, T.; Malola, S.; Takano, S.; Niihori, Y.; Kurashige, W.; Yamazoe, S.; Tsukuda, T.; Häkkinen, H. A Critical Size for Emergence of Nonbulk Electronic and Geometric Structures in Dodecanethiolate-Protected Au Clusters. *J. Am. Chem. Soc.* **2015**, 137, 1206–1212.
- (28) Weerawardene, K. L. D. M.; Aikens, C. M. Theoretical Insights into the Origin of Photoluminescence of $\mathrm{Au}_{25}(\mathrm{SR})_{18}^{}$ Nanoparticles. *J. Am. Chem. Soc.* **2016**, 138, 11202–11210.
- (29) Senanayake, R. D.; Guidez, E. B.; Neukirch, A. J.; Prezhdo, O. V.; Aikens, C. M. Theoretical Investigation of Relaxation Dynamics in Au₃₈(SH)₂₄ Thiolate-Protected Gold Nanoclusters. *J. Phys. Chem. C* **2018**, *122*, 16380–16388.
- (30) Senanayake, R. D.; Akimov, A. V.; Aikens, C. M. Theoretical Investigation of Electron and Nuclear Dynamics in the $[\mathrm{Au}_{25}(\mathrm{SH})_{18}]^{-1}$ Thiolate-Protected Gold Nanocluster. *J. Phys. Chem.* C **2017**, 121, 10653–10662.
- (31) Ma, Z.; Wang, P.; Pei, Y. Geometric Structure, Electronic Structure and Optical Absorption Properties of One-dimensional Thiolate-protected Gold Clusters Containing a Quasi-face-centered-cubic (quasi-fcc) Au-core: a Density-functional Theoretical Study. *Nanoscale* **2016**, *8*, 17044–17054.
- (32) Tang, Q.; Hu, G.; Fung, V.; Jiang, D.-e. Insights into Interfaces, Stability, Electronic Properties, and Catalytic Activities of Atomically Precise Metal Nanoclusters from First Principles. *Acc. Chem. Res.* **2018**, *51*, 2793–2802.
- (33) Pei, Y.; Wang, P.; Ma, Z.; Xiong, L. Growth-Rule-Guided Structural Exploration of Thiolate-Protected Gold Nanoclusters. *Acc. Chem. Res.* **2019**, *52*, 23–33.
- (34) Malola, S.; Lehtovaara, L.; Enkovaara, J.; Häkkinen, H. Birth of the Localized Surface Plasmon Resonance in Monolayer-Protected Gold Nanoclusters. *ACS Nano* **2013**, *7*, 10263–10270.
- (35) Weissker, H. C.; Escobar, H. B.; Thanthirige, V. D.; Kwak, K.; Lee, D.; Ramakrishna, G.; Whetten, R. L.; López-Lozano, X. Information on Quantum States Pervades the Visible Spectrum of the Ubiquitous Au₁₄₄(SR)₆₀ Gold Nanocluster. *Nat. Commun.* **2014**, *5*, 3785.
- (36) Varnavski, O.; Ramakrishna, G.; Kim, J.; Lee, D.; Goodson, T. Critical Size for the Observation of Quantum Confinement in Optically Excited Gold Clusters. *J. Am. Chem. Soc.* **2010**, *132*, 16–17.
- (37) Devadas, M. S.; Bairu, S.; Qian, H.; Sinn, E.; Jin, R.; Ramakrishna, G. Temperature-Dependent Optical Absorption Properties of Monolayer-Protected Au₂₅ and Au₃₈ Clusters. *J. Phys. Chem. Lett.* **2011**, *2*, 2752–2758.
- (38) Kwak, K.; Thanthirige, V. D.; Pyo, K.; Lee, D.; Ramakrishna, G. Energy Gap Law for Exciton Dynamics in Gold Cluster Molecules. *J. Phys. Chem. Lett.* **2017**, *8*, 4898–4905.
- (39) Stoll, T.; Sgrò, E.; Jarrett, J. W.; Réhault, J.; Oriana, A.; Sala, L.; Branchi, F.; Cerullo, G.; Knappenberger, K. L. Superatom State-Resolved Dynamics of the Au₂₅(SC₈H₉)₁₈ Cluster from Two-Dimensional Electronic Spectroscopy. *J. Am. Chem. Soc.* **2016**, *138*, 1788–1791.
- (40) Green, T. D.; Herbert, P. J.; Yi, C.; Zeng, C.; McGill, S.; Jin, R.; Knappenberger, K. L. Characterization of Emissive States for Structurally Precise $Au_{25}(SC_8H_9)_{18}{}^0$ Monolayer-Protected Gold Nanoclusters Using Magnetophotoluminescence Spectroscopy. *J. Phys. Chem. C* **2016**, *120*, 17784–17790.
- (41) Herbert, P. J.; Mitra, U.; Knappenberger, K. L. Variable-temperature Variable-field Magnetic Circular Photoluminescence (VTVH-MCPL) Spectroscopy for Electronic-structure Determination in Nanoscale Chemical Systems. *Opt. Lett.* **2017**, *42*, 4833–4836.
- (42) Mustalahti, S.; Myllyperkiö, P.; Lahtinen, T.; Salorinne, K.; Malola, S.; Koivisto, J.; Häkkinen, H.; Pettersson, M. Ultrafast Electronic Relaxation and Vibrational Cooling Dynamics of Au₁₄₄(SC₂H₄Ph)₆₀ Nanocluster Probed by Transient Mid-IR Spectroscopy. *J. Phys. Chem. C* **2014**, *118*, 18233–18239.
- (43) Mustalahti, S.; Myllyperkiö, P.; Malola, S.; Lahtinen, T.; Salorinne, K.; Koivisto, J.; Häkkinen, H.; Pettersson, M. Molecule-like Photodynamics of Au₁₀₂(pMBA)₄₄ Nanocluster. *ACS Nano* **2015**, *9*, 2328–2335.

- (44) Stamplecoskie, K. G.; Kamat, P. V. Size-Dependent Excited State Behavior of Glutathione-Capped Gold Clusters and Their Light-Harvesting Capacity. *J. Am. Chem. Soc.* **2014**, *136*, 11093–11099.
- (45) Stamplecoskie, K. G.; Yousefalizadeh, G.; Gozdzialski, L.; Ramsay, H. Photovoltaics as an Experimental Tool for Determining Frontier Orbital Energies and Photocatalytic Activity of Thiol Protected Gold Clusters. *J. Phys. Chem. C* 2018, 122, 13738–13744. (46) Yu, Y.; Luo, Z.; Chevrier, D. M.; Leong, D. T.; Zhang, P.; Jiang,
- D.-e.; Xie, J. Identification of a Highly Luminescent Au₂₂(SG)₁₈ Nanocluster. *J. Am. Chem. Soc.* **2014**, *136*, 1246–1249.
- (47) Pyo, K.; Thanthirige, V. D.; Kwak, K.; Pandurangan, P.; Ramakrishna, G.; Lee, D. Ultrabright Luminescence from Gold Nanoclusters: Rigidifying the Au(I)—Thiolate Shell. *J. Am. Chem. Soc.* **2015**, *137*, 8244—8250.
- (48) Nieto-Ortega, B.; Bürgi, T. Vibrational Properties of Thiolate-Protected Gold Nanoclusters. Acc. Chem. Res. 2018, 51, 2811–2819.
- (49) Knoppe, S.; Bürgi, T. Chirality in Thiolate-Protected Gold Clusters. Acc. Chem. Res. 2014, 47, 1318–1326.
- (50) Philip, R.; Chantharasupawong, P.; Qian, H.; Jin, R.; Thomas, J. Evolution of Nonlinear Optical Properties: From Gold Atomic Clusters to Plasmonic Nanocrystals. *Nano Lett.* **2012**, *12*, 4661–4667.
- (51) Kreibig, U.; Vollmer, M. Optical Properties of Metal Clusters; Springer: Berlin, 1995.
- (52) Chang, S.-S.; Shih, C.-W.; Chen, C.-D.; Lai, W.-C.; Wang, C. R. C. The Shape Transition of Gold Nanorods. *Langmuir* **1999**, *15*, 701–709.
- (53) Jin, R. Quantum Sized, Thiolate-Protected Gold Nanoclusters. *Nanoscale* **2010**, *2*, 343–362.
- (54) Qian, H.; Eckenhoff, W. T.; Zhu, Y.; Pintauer, T.; Jin, R. Total Structure Determination of Thiolate-Protected Au₃₈ Nanoparticles. *J. Am. Chem. Soc.* **2010**, *132*, 8280–8281.
- (55) Das, A.; Li, T.; Nobusada, K.; Zeng, C.; Rosi, N. L.; Jin, R. Nonsuperatomic $[Au_{23}(SC_6H_{11})_{16}]^-$ Nanocluster Featuring Bipyramidal Au_{15} Kernel and Trimeric $Au_3(SR)_4$ Motif. *J. Am. Chem. Soc.* **2013**, *135*, 18264–18267.
- (56) Das, A.; Li, T.; Li, G.; Nobusada, K.; Zeng, C.; Rosi, N. L.; Jin, R. Crystal Structure and Electronic Properties of a Thiolate-protected Au₂₄ Nanocluster. *Nanoscale* **2014**, *6*, 6458–6462.
- (57) Zeng, C.; Chen, Y.; Iida, K.; Nobusada, K.; Kirschbaum, K.; Lambright, K. J.; Jin, R. Gold Quantum Boxes: On the Periodicities and the Quantum Confinement in the Au₂₈, Au₃₆, Au₄₄, and Au₅₂ Magic Series. *J. Am. Chem. Soc.* **2016**, *138*, 3950–3953.
- (58) Zhou, M.; Zeng, C.; Sfeir, M. Y.; Cotlet, M.; Iida, K.; Nobusada, K.; Jin, R. Evolution of Excited-State Dynamics in Periodic Au₂₈, Au₃₆, Au₄₄, and Au₅₂ Nanoclusters. *J. Phys. Chem. Lett.* **2017**, *8*, 4023–4030.
- (59) Yi, C.; Zheng, H.; Herbert, P. J.; Chen, Y.; Jin, R.; Knappenberger, K. L. Ligand- and Solvent-Dependent Electronic Relaxation Dynamics of Au₂₅(SR)₁₈ Monolayer-Protected Clusters. *J. Phys. Chem. C* **2017**, *121*, 24894–24902.
- (60) Zeng, C.; Chen, Y.; Li, G.; Jin, R. Magic Size $Au_{64}(S-c-C_6H_{11})_{32}$ Nanocluster Protected by Cyclohexanethiolate. *Chem. Mater.* **2014**, 26, 2635–2641.
- (61) Zeng, C.; Liu, C.; Chen, Y.; Rosi, N. L.; Jin, R. Atomic Structure of Self-Assembled Monolayer of Thiolates on a Tetragonal Au₉₂ Nanocrystal. *J. Am. Chem. Soc.* **2016**, *138*, 8710–8713.
- (62) Li, G.; Zeng, C.; Jin, R. Thermally Robust Au₉₉(SPh)₄₂ Nanoclusters for Chemoselective Hydrogenation of Nitrobenzaldehyde Derivatives in Water. *J. Am. Chem. Soc.* **2014**, *136*, 3673–3679.
- (63) Liao, L.; Chen, J.; Wang, C.; Zhuang, S.; Yan, N.; Yao, C.; Xia, N.; Li, L.; Bao, X.; Wu, Z. Transition-sized Au₉₂ Nanoparticle Bridging Non-fcc-structured Gold Nanoclusters and fcc-structured Gold Nanocrystals. *Chem. Commun.* **2016**, *52*, 12036–12039.
- (64) Nimmala, P. R.; Dass, A. Au₉₉(SPh)₄₂ Nanomolecules: Aromatic Thiolate Ligand Induced Conversion of Au₁₄₄(SCH₂CH₂Ph)₆₀. J. Am. Chem. Soc. **2014**, 136, 17016–17023.
- (65) Higaki, T.; Liu, C.; Zhou, M.; Luo, T. Y.; Rosi, N. L.; Jin, R. Tailoring the Structure of 58-Electron Gold Nanoclusters: Au₁₀₃S₂(S-

- Nap)₄₁ and Its Implications. J. Am. Chem. Soc. 2017, 139, 9994–10001
- (66) Chen, Y.; Zeng, C.; Liu, C.; Kirschbaum, K.; Gayathri, C.; Gil, R. R.; Rosi, N. L.; Jin, R. Crystal Structure of Barrel-Shaped Chiral Au₁₃₀(p-MBT)₅₀ Nanocluster. *J. Am. Chem. Soc.* **2015**, *137*, 10076–10079
- (67) Zeng, C.; Chen, Y.; Kirschbaum, K.; Lambright, K. J.; Jin, R. Emergence of Hierarchical Structural Complexities in Nanoparticles and Their Assembly. *Science* **2016**, 354, 1580–1584.
- (68) Padelford, J. W.; Zhou, M.; Chen, Y.; Jin, R.; Wang, G. Electronic Transitions in Highly Symmetric Au₁₃₀ Nanoclusters by Spectroelectrochemistry and Ultrafast Spectroscopy. *J. Phys. Chem. C* **2017**, *121*, 21217–21224.
- (69) Zhou, M.; Zeng, C.; Song, Y.; Padelford, J. W.; Wang, G.; Sfeir, M. Y.; Higaki, T.; Jin, R. On the Non-Metallicity of 2.2 nm Au₂₄₆(SR)₈₀ Nanoclusters. *Angew. Chem., Int. Ed.* **2017**, 56, 16257–16261.
- (70) Higaki, T.; Zhou, M.; Lambright, K. J.; Kirschbaum, K.; Sfeir, M. Y.; Jin, R. Sharp Transition from Nonmetallic Au₂₄₆ to Metallic Au₂₇₉ with Nascent Surface Plasmon Resonance. *J. Am. Chem. Soc.* **2018**, *140*, 5691–5695.
- (71) Aruda, K. O.; Tagliazucchi, M.; Sweeney, C. M.; Hannah, D. C.; Schatz, G. C.; Weiss, E. A. Identification of Parameters through Which Surface Chemistry Determines the Lifetimes of Hot Electrons in Small Au Nanoparticles. *Proc. Natl. Acad. Sci. U. S. A.* **2013**, *110*, 4212–4217.
- (72) Link, S.; El-Sayed, M. A. Optical Properties and Ultrafast Dynamics of Metallic Nanocrystals. *Annu. Rev. Phys. Chem.* **2003**, *54*, 331–366.
- (73) Higaki, T.; Zhou, M.; He, G.; House, S. D.; Sfeir, M. Y.; Yang, J. C.; Jin, R. Anomalous Phonon Relaxation in Au₃₃₃(SR)₇₉ Nanoparticles with Nascent Plasmons. *Proc. Natl. Acad. Sci. U. S. A.* **2019**, *116*, 13215–13220.
- (74) Englman, R.; Jortner, J. Energy gap law for radiationless transitions in large molecules. *Mol. Phys.* **1970**, *18*, 145–164.
- (75) Varnavski, O.; Ramakrishna, G.; Kim, J.; Lee, D.; Goodson, T., III Optically Excited Acoustic Vibrations in Quantum-Sized Monolayer-Protected Gold Clusters. *ACS Nano* **2010**, *4*, 3406–3412.
- (76) Zhou, M.; Jin, R.; Sfeir, M. Y.; Chen, Y.; Song, Y.; Jin, R. Electron Localization in Rod-shaped Triicosahedral Gold Nanocluster. *Proc. Natl. Acad. Sci. U. S. A.* 2017, 114, E4697—E4705.
- (77) Maioli, P.; Stoll, T.; Sauceda, H. E.; Valencia, I.; Demessence, A.; Bertorelle, F.; Crut, A.; Vallée, F.; Garzón, I. L.; Cerullo, G.; Del Fatti, N. Mechanical Vibrations of Atomically Defined Metal Clusters: From Nano- to Molecular-Size Oscillators. *Nano Lett.* **2018**, *18*, 6842–6849.